Control and Cybernetics

vol. **47** (2018) No. 3

Design of an adaptive fuzzy variable structure compensator for the nonholonomic mobile robot in trajectory tracking task*

by

Mauricio Begnini[1], Douglas Wildgrube Bertol[2] and Nardênio Almeida Martins[1,3]

[1]Departamento de Informática, Universidade Estadual de Maringá - UEM, Programa de Pós-Graduação em Ciência da Computação, Avenida Colombo, 5790, 87020-900, Maringá, PR, Brasil
pg4937@uem.br, namartin@din.uem.br
[2]Departamento de Engenharia Elétrica, Universidade do Estado de Santa Catarina - UDESC, Rua Paulo Malschitzki, s/numero, 89219-710, Joinville, SC, Brasil
douglas.bertol@udesc.br
[3]Universidade Federal de Santa Catarina - UFSC, Departamento de Automação e Sistemas, Grupo de Pesquisa Robótica, Caixa Postal 476, 88040-900, Florianópolis, SC, Brasil
nardenio@das.ufsc.br - Corresponding author

Abstract: A robust adaptive kinematic control strategy, based on the methodology of variable structure control is considered in this paper. Because the dynamics of mobile robots is subject to uncertainties and disturbances, a fuzzy compensator is adopted to estimate them. In order to minimize the tracking errors and to attenuate the chattering phenomenon, an adaptation law for the fuzzy compensator is obtained by Lyapunov stability theory so as to asymptotically stabilize the control system as well as guarantee the convergence of the tracking errors. In terms of comparison with the boundary layer variable structure controller, simulations and experiments verify the feasibility and effectiveness of the proposed kinematic control strategy for the nonholonomic mobile robots under the incidence of uncertainties and disturbances.

Keywords: nonholonomic mobile robots, trajectory tracking, variable structure control, uncertainties and disturbances, fuzzy compensator, Lyapunov theory

*Submitted: April 2017; Accepted: November 2018

1. Introduction

Variable structure systems (VSS) theory offers great advantages over the traditional linear approach in terms of robustness and efficiency (see Utkin, Guldner and Shi, 2009). The variable structure control (VSC) and, in particular, the popular sliding mode control (SMC), provide a robust nonlinear feedback control technique that utilizes discontinuous control actions to have the system state reach and thereafter stay within some predefined sliding regime. In sliding mode, all state trajectories are confined to the sliding regime, and system responses then completely depend on the characteristics of the sliding regime. However, before the sliding motion occurs, there usually exists a reaching phase, during which the invariance property of the sliding mode is not guaranteed. The existence of such a reaching phase deteriorates the performance robustness. Moreover, the discontinuous control actions may excite unmodeled dynamics and lead to oscillations in the state vector at finite frequencies. These oscillations, normally referred to as chatter, are known to result in low control accuracy, high heat loss in electric power circuits and excessive wear of the moving mechanical parts, see Utkin (1993). The chattering phenomenon is thus a serious implementation drawback.

It should also be emphasized that uncertainties and disturbances are inevitable in practice and the dynamics of nonholonomic mobile robots is subject to them. The respective phenomena must have a known boundary in order to guarantee the stability of the closed-loop control system (Utkin, Guldner and Shi, 2009). However, such an assumption is not mild, because the boundary value can hardly be exactly known in advance. The lack of the boundary value may cause several drawbacks, such as deficiency of the system stability, decrease of the system robustness and deterioration of the system performance. In order to take VSC and SMC into account for the trajectory tracking control problem, it is necessary to minimize and compensate for the uncertainties and disturbances.

With the advent of artificial intelligence systems, there have been increasing efforts to improve VSC and SMC performance by integrating fuzzy logic systems. This approach has emerged as a promising one for dealing with uncertain nonlinear systems and for relieving VSC implementation difficulties (see Kaynak, Erbatur and Ertugner, 2001), i.e., the methodology of fuzzy logic can effectively handle complex nonlinear systems with uncertainties and disturbances (Farrel and Polycarpou, 2006).

By integrating adaptation techniques into the fuzzy sliding mode controls, the adaptive fuzzy sliding mode control schemes (see Erbatur and Kaynak, 2001; Guo and Woo, 2003; Wai, 2007; Kung, Chen and Kung, 2005; Kung and Chen, 2007) gain several excellent features, such as their adaptability and chatter alleviation, although convergence of the tracking error can be slow due to the adaptation mechanisms, leading to poor transient responses. Thus, in order to circumvent the uncertainties and disturbances of the VSC-based control problem, this paper proposes a fuzzy inference system, as an alternative choice, to

compensate for them and to attenuate the tracking errors and chattering phenomenon. The fuzzy system has to adaptively approximate the uncertainties and disturbances, because the assumption that they have an unknown boundary holds true. The fuzzy compensator and the variable structure controller work in parallel to achieve the trajectory tracking. The VSC law and the robust adaptation law are derived from the Lyapunov's direct method.

The feasibility and robustness of the proposed adaptive fuzzy variable structure control (AFVSC), applied to a nonholonomic mobile robot, are verified by means of simulations and experimental tests. In comparison with the results obtained via the boundary layer variable structure controller (VSCBL), the proposed AFVSC can also improve the tracking performance. The benefit of the AFVSC is that it is only subject to the mild assumption that the uncertainties and disturbances have an unknown boundary. Moreover, in the results obtained from simulations and experimental tests it is verified that the loss of invariance has little practical meaning (see Wang and Gao, 1995) and the robustness is ensured in the case of the AFVSC. An extension of some of the results, presented here, can be found in Begnini, Bertol and Martins (2017).

This paper is organized as follows. Section 2 presents the kinematic and dynamic models for DWMRs, and the description of the trajectory tracking control problem. The kinematic and dynamic controllers of the DWMRs are summarized in Section 3. In Section 4 the proposed AFVSC methodology, based on the classical VSC and VSCBL, is presented. Section 5 shows the simulation results and real-time experiments, and Section 6 presents the conclusions.

2. Problem formulation

In this section we present the kinematic and dynamic models for a DWMR, and the control problem to be resolved.

2.1. Kinematics and dynamics of DWMRs

A simple model that represents the essentials of the kinematics and dynamics of the DWMR is extensively used in literature (see, e.g., Park et al., 2009; Elyoussef et al., 2014; or Martins et al., 2015). Disregarding gravitational forces ($\boldsymbol{G}(\boldsymbol{q}) = \boldsymbol{0}$) and considering uncertainties and disturbances, the posture dynamic and kinematic models of DWMRs for control purposes are defined as:

$$\dot{\boldsymbol{q}} = \boldsymbol{S}(\boldsymbol{q})\boldsymbol{v}, \tag{1}$$

$$\bar{\boldsymbol{M}}(\boldsymbol{q})\dot{\boldsymbol{v}} + \bar{\boldsymbol{C}}(\boldsymbol{q},\dot{\boldsymbol{q}})\boldsymbol{v} + \boldsymbol{\delta}_{\mathrm{d}}(\boldsymbol{q},\boldsymbol{v}) = \bar{\boldsymbol{D}}(\boldsymbol{q})\boldsymbol{\tau}, \tag{2}$$

where $\boldsymbol{q}$ is the posture vector in the plane, $\boldsymbol{v} = [\nu\ \omega]^{\mathrm{T}}$ is the velocity vector, with longitudinal velocity (ν), and rotational velocity (ω), $\boldsymbol{\tau}$ is the torque vector,

$$\bar{\boldsymbol{M}}(\boldsymbol{q}) = \boldsymbol{S}^{\mathrm{T}}(\boldsymbol{q})\boldsymbol{M}(\boldsymbol{q})\boldsymbol{S}(\boldsymbol{q}),$$

$$\bar{\boldsymbol{C}}(\boldsymbol{q},\dot{\boldsymbol{q}}) = \boldsymbol{S}^{\mathrm{T}}(\boldsymbol{q})\boldsymbol{M}(\boldsymbol{q})\dot{\boldsymbol{S}}(\boldsymbol{q},\dot{\boldsymbol{q}}) + \boldsymbol{S}^{\mathrm{T}}(\boldsymbol{q})\boldsymbol{C}(\boldsymbol{q},\dot{\boldsymbol{q}})\boldsymbol{S}(\boldsymbol{q}),$$

$$\bar{\boldsymbol{D}}(\boldsymbol{q}) = \boldsymbol{S}^{\mathrm{T}}(\boldsymbol{q})\boldsymbol{D}(\boldsymbol{q})$$

(see, e.g., Park et al., 2009; Elyoussef et al., 2014; or Martins et al., 2015), and

$$\boldsymbol{\delta}_{\mathrm{d}}(\boldsymbol{q}, \dot{\boldsymbol{q}}, \boldsymbol{v}, \dot{\boldsymbol{v}}, t) = \Delta\bar{\boldsymbol{M}}(\boldsymbol{q})\dot{\boldsymbol{v}} + \Delta\bar{\boldsymbol{C}}(\boldsymbol{q}, \dot{\boldsymbol{q}})\boldsymbol{v} + \bar{\boldsymbol{\tau}}_{\mathrm{p}}, \tag{3}$$

where $\Delta\bar{\boldsymbol{M}}(\boldsymbol{q})$ and $\Delta\bar{\boldsymbol{C}}(\boldsymbol{q}, \dot{\boldsymbol{q}})$ denote unknown internal uncertainties, including both parametric and non-parametric uncertainties, and $\bar{\boldsymbol{\tau}}_{\mathrm{p}} = \boldsymbol{S}^{\mathrm{T}}(\boldsymbol{q})\boldsymbol{\tau}_{\mathrm{p}}$ denotes uncertainties and disturbances, including friction (Park et al., 2009). The Jacobian matrix $\boldsymbol{S}(\boldsymbol{q})$, the nominal matrix of inertia $\boldsymbol{M}(\boldsymbol{q})$, Coriolis and centrifugal matrix $\boldsymbol{C}(\boldsymbol{q}, \dot{\boldsymbol{q}})$, and input transformation matrix $\boldsymbol{D}(\boldsymbol{q})$ are provided in Elyoussef et al. (2014), as being representative of the PowerBot DWMR.

2.2. Problem statement

The trajectory tracking control problem for DWMRs (Fierro and Lewis, 1998) is established by proposing a control structure that uses adaptation and fuzzy logic on VSC, in order to design a robust kinematic controller that avoids chattering and makes the posture tracking errors tend to zero quickly, and a PD control as the principle of a dynamic controller that makes the auxiliary velocity tracking errors also tend to zero quickly.

3. Control project

Let the control synthesis be treated separately, namely, we shall present first the design of the dynamic control and then the design of the kinematic control.

3.1. Dynamic control

The objective of the dynamic controller is to compensate for the known torques and forces, described in Eq. (2), and ensure fast convergence of the auxiliary velocity tracking errors $\boldsymbol{v}_{\mathrm{e}} = \boldsymbol{v}_{\mathrm{c}} - \boldsymbol{v}$ to zero. As the uncertainties $\boldsymbol{\delta}_d$ are unknown, they are set to zero for the purpose of this design, and will be considered just for adjusting control gains and in the design of the kinematic controller. Now, we consider the calculus of the PD control, similar to that in Spong, Hutchinson and Vidgasagar (2006), i.e.,

$$\bar{\boldsymbol{u}} = \begin{bmatrix} \bar{u}_{\nu}(s) \\ \bar{u}_{\omega}(s) \end{bmatrix} = \begin{bmatrix} \mathrm{k}_{\mathrm{p}_{\nu}} & 0 \\ 0 & \mathrm{k}_{\mathrm{p}_{\omega}} \end{bmatrix} \boldsymbol{v}_{\mathrm{e}} + \begin{bmatrix} \mathrm{k}_{\mathrm{d}_{\nu}} & 0 \\ 0 & \mathrm{k}_{\mathrm{d}_{\omega}} \end{bmatrix} \dot{\boldsymbol{v}}_{\mathrm{e}}, \tag{4}$$

where $\boldsymbol{v}_{\mathrm{e}} = \boldsymbol{v}_{\mathrm{c}} - \boldsymbol{v}$ is the error between the control velocity $\boldsymbol{v}_{\mathrm{c}}$ and velocity of the DWMR $\boldsymbol{v}$, and

$$\boldsymbol{\tau} = \bar{\boldsymbol{D}}(\boldsymbol{q})^{-1}\bar{\boldsymbol{u}}. \tag{5}$$

is the control law.

The vector $\bar{\boldsymbol{u}} = [\bar{u}_{\nu}\ \bar{u}_{\omega}]^{\mathrm{T}}$ is a new control input, where the proportional gains $\mathrm{k}_{\mathrm{p}_{\nu}}$, $\mathrm{k}_{\mathrm{p}_{\omega}}$ and the derivative gains $\mathrm{k}_{\mathrm{d}_{\nu}}$, $\mathrm{k}_{\mathrm{d}_{\omega}}$ should be designed to achieve fast

convergence of $\boldsymbol{v}_{\mathrm{e}}$, as can be seen in Elyoussef et al. (2014). The stability analysis of this controller is similar to the ones in Spong, Hutchinson and Vidgasagar (2006).

Further, the authors of this work are aware that the VSCBL or AFVSC could handle the entire control problem without the PD controller, but as the real DWMR that is used as experimental platform (the PowerBot DWMR) has in its firmware this PD controller as a basic and irremovable dynamic control in the architecture (the DWMR cannot be directly torque controlled), the approach applied has to reflect this architecture in the simulations and in the entire solution.

3.2. Kinematic control

The kinematics of the virtual DWMR is modeled as:

$$\dot{\boldsymbol{q}}_{\mathrm{r}} = \boldsymbol{S}(\boldsymbol{q}_{\mathrm{r}})\boldsymbol{v}_{\mathrm{r}}, \qquad \dot{x}_{\mathrm{r}} = \nu_{\mathrm{r}}\cos(\theta_{\mathrm{r}}), \qquad \dot{y}_{\mathrm{r}} = \nu_{\mathrm{r}}\sin(\theta_{\mathrm{r}}), \qquad \dot{\theta}_{\mathrm{r}} = \omega_{\mathrm{r}}, \tag{6}$$

where $\boldsymbol{q}_{\mathrm{r}} = [x_{\mathrm{r}}\ y_{\mathrm{r}}\ \theta_{\mathrm{r}}]^{\mathrm{T}}$ is the reference posture vector of the virtual DWMR, and $\boldsymbol{v}_{\mathrm{r}} = [\nu\ \omega]^{\mathrm{T}}$ is the reference velocity vector of the virtual DWMR.

Converting the posture tracking errors in the inertial frame to the DWMR frame, the posture error equation of the DWMR can be written down as (see Kanayama et al., 1991)

$$\boldsymbol{q}_{\mathrm{e}} = \begin{bmatrix} x_{\mathrm{e}} \\ y_{\mathrm{e}} \\ \theta_{\mathrm{e}} \end{bmatrix} = \begin{bmatrix} \cos\theta_{\mathrm{r}} & \sin\theta_{\mathrm{r}} & 0 \\ -\sin\theta_{\mathrm{r}} & \cos\theta_{\mathrm{r}} & 0 \\ 0 & 0 & 1 \end{bmatrix} \begin{bmatrix} x_{\mathrm{r}} - x \\ y_{\mathrm{r}} - y \\ \theta_r - \theta \end{bmatrix}, \tag{7}$$

and, consequently, the error dynamics of the closed-loop system for trajectory tracking is obtained from the time derivative of Eq. (7), after mathematical manipulations, as:

$$\dot{x}_{\mathrm{e}} = \omega y_{\mathrm{e}} - \nu + \nu_{\mathrm{r}}\cos\theta_{\mathrm{e}}, \qquad \dot{y}_{\mathrm{e}} = -\omega x_{\mathrm{e}} + \nu_{\mathrm{r}}\sin\theta_{\mathrm{e}}, \qquad \dot{\theta}_{\mathrm{e}} = \omega_{\mathrm{r}} - \omega. \tag{8}$$

Under robustness considerations, in practical situations, the velocities and the tracking errors are not equal to zero. The best that can be done is to guarantee that the error converges to a neighborhood of the origin. If uncertainties and disturbances (e.g., external disturbances) drive the system away from the compact convergence set, the derivative of the Lyapunov function becomes negative and the energy of the system decreases uniformly; therefore, the error becomes small again (Fierro and Lewis, 1998).

As perfect velocity tracking does not hold in practice, the dynamic controller generates auxiliary velocity tracking errors $\boldsymbol{v}_{\mathrm{e}}$, which are bounded by some known constant. These tracking errors can be seen as an uncertainty and disturbance for the kinematic model (see Fig. 1). The closed-loop kinematic model becomes:

$$\dot{x} = (\nu_{\mathrm{c}} + \nu_{\mathrm{e}})\cos\theta, \qquad \dot{y} = (\nu_{\mathrm{c}} + \nu_{\mathrm{e}})\sin\theta, \qquad \dot{\theta} = (\omega_{\mathrm{c}} + \omega_{\mathrm{e}}), \tag{9}$$

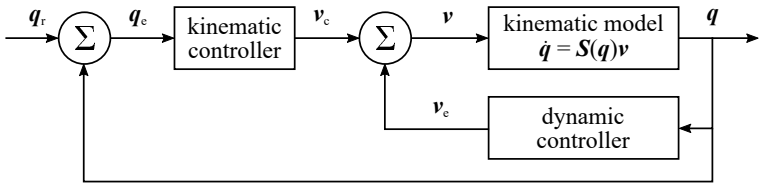

Figure 1. Block diagram of the closed-loop control system: $\boldsymbol{v}_\mathrm{e}$ as uncertainty and disturbance for the kinematic model (similar to that of Fierro and Lewis, 1998)

where $\boldsymbol{v}_\mathrm{e} = [\nu_\mathrm{e}\ \omega_\mathrm{e}]^\mathrm{T}$ and $\boldsymbol{v}_\mathrm{c} = [\nu_\mathrm{c}\ \omega_\mathrm{c}]^\mathrm{T}$ denote the auxiliary velocity tracking errors and the desired velocity control inputs, respectively. The uncertainty and disturbance, given by $\boldsymbol{v}_\mathrm{e}$, satisfies the matching condition, i.e., the nonholonomic constraint $\dot{y}\cos\theta - \dot{x}\sin\theta = 0$ is not violated. Then, by using standard Lyapunov methods, it can be shown that along a system's solution, $|\boldsymbol{q}_\mathrm{e}|$ is bounded, and thus $|\dot{\boldsymbol{q}}_\mathrm{e}|$ is also bounded. The norm of the auxiliary velocity tracking errors affects directly the norm of the posture tracking errors. Note that the norm of the auxiliary velocity tracking errors $|\boldsymbol{v}_\mathrm{e}|$ depends on the proportional gains, $\mathrm{k}_{\mathrm{p}_\nu}$ and $\mathrm{k}_{\mathrm{p}_\omega}$, and the derivative gains, $\mathrm{k}_{\mathrm{d}_\nu}$ and $\mathrm{k}_{\mathrm{d}_\omega}$, see Eq. (4). Since $|\boldsymbol{v}_\mathrm{e}|$ can be made arbitrarily small, then $|\boldsymbol{q}_\mathrm{e}|$ can also be made arbitrarily small (Fierro and Lewis, 1998).

The effect of the uncertainties and disturbances (e. g., external disturbances) that affect the system can be considered, after mathematical manipulations, as a term:

$$\boldsymbol{\delta}_\mathrm{k}(\boldsymbol{q}, t) = [\omega_\mathrm{e} y_\mathrm{e} - \nu_\mathrm{e} \quad -\omega_\mathrm{e} x_\mathrm{e} \quad -\omega_\mathrm{e}]^\mathrm{T}, \tag{10}$$

added to the right hand side of error dynamics, Eq. (8). Now, recalling the invariance principle for VSC, described by Utkin, Guldner and Shi (2009), and assuming that the $\boldsymbol{\delta}_\mathrm{k}(\boldsymbol{q}, t)$ is matched by the control signal $\boldsymbol{v}_\mathrm{c}$, one can conclude that if the system, Eq. (8), is enforced to a sliding motion under some desired constraints, it will be ideally invariant to $\boldsymbol{\delta}_\mathrm{k}(\boldsymbol{q}, t)$ in Eq. (10).

For purposes of designing the kinematic controller, which is based on VSC theory, from the error dynamics, Eq. (8), the following sliding surfaces are selected:

$$\boldsymbol{\sigma}(\tilde{\boldsymbol{z}}, t) = \begin{bmatrix}\sigma_1 \\ \sigma_2\end{bmatrix} = \begin{bmatrix}\Lambda_1 x_\mathrm{e} \\ \Lambda_2 y_\mathrm{e} + \Lambda_3 \theta_\mathrm{e}\end{bmatrix}, \tag{11}$$

$$\boldsymbol{\sigma}^*(\tilde{\boldsymbol{z}}, t) = \boldsymbol{B}_{0_\sigma}^\mathrm{T} \boldsymbol{\sigma}(\tilde{\boldsymbol{z}}, t) = \boldsymbol{B}_{0_\sigma}^\mathrm{T} \boldsymbol{\Lambda}^\mathrm{T} \tilde{\boldsymbol{z}}, \tag{12}$$

where $\Lambda_1, \Lambda_2, \Lambda_3$ are positive constants, and $\boldsymbol{B}_{0_\sigma}$ is defined as in Martins et al. (2015). It should be emphasized that the selection of the sliding surfaces is a critical and difficult problem for the VSC design, due to the posture error, Eq. (7), representing a nonlinear system of multiple inputs (see Lee et al., 2009).

After the selection of the sliding surfaces and with reference to the generic modeling of nonlinear systems relative to the VSC design, the error dynamics in Eq. (8) can be rewritten as:

$$\dot{\tilde{\boldsymbol{z}}} = \boldsymbol{A}_0(\tilde{\boldsymbol{z}}, t) + \boldsymbol{B}_0(\tilde{\boldsymbol{z}}, t)\boldsymbol{v}(\tilde{\boldsymbol{z}}, t) + \boldsymbol{d}_{\mathrm{b}}(t), \tag{13}$$

since there are no parametric uncertainties and $\boldsymbol{z}$, $\boldsymbol{A}_0$, $\boldsymbol{B}_0$, $\boldsymbol{d}_{\mathrm{b}}$ are defined as in Martins et al. (2015).

For the stability analysis, the Lyapunov function candidate is chosen in the form:

$$V = \frac{1}{2}\boldsymbol{\sigma}^{\mathrm{T}}\boldsymbol{\sigma}, \tag{14}$$

which is positive definite. The sliding surface will be attractive, since the control law $\boldsymbol{v}$, defined as,

$$\boldsymbol{v} = -\boldsymbol{B}_{0_\sigma}^{-1}\boldsymbol{A}_{0_\sigma} - \mathbf{G}sign(\boldsymbol{\sigma}^*) - \mathbf{K}\boldsymbol{\sigma}^*, \tag{15}$$

ensures that

$$\dot{V} = \boldsymbol{\sigma}^{\mathrm{T}}\dot{\boldsymbol{\sigma}} = -{\boldsymbol{\sigma}^*}^{\mathrm{T}}\mathbf{G}sign(\boldsymbol{\sigma}^*) - {\boldsymbol{\sigma}^*}^{\mathrm{T}}\mathbf{K}\boldsymbol{\sigma}^* + {\boldsymbol{\sigma}^*}^{\mathrm{T}}\tilde{\boldsymbol{d}}_0, \tag{16}$$

is negative definite. The definitions of the vectors $\boldsymbol{A}_{0_\sigma}$, $\tilde{\boldsymbol{d}}_0$ and matrices $\mathbf{G}$, $\mathbf{K}$, as well as further details on control law and stability analysis can be found in Martins et al. (2015).

4. Control design considering chattering attenuation

4.1. Preliminaries

Unfortunately, in practical implementation, due to delays, neglected dynamics, sampling frequency limitation, physical limitations of actuators and imperfections of switching, it is not possible to switch the control from a value to another one instantaneously (see Martins et al., 2010; Elyoussef et al., 2014). Thus, the state trajectory fluctuates in the vicinity of the sliding surface, instead of sliding over it. This phenomenon, known as chattering, can be avoided or at least reduced by replacing the discontinuous function $sign(\boldsymbol{\sigma}^*)$ by its continuous approximation. A commonly used solution is the use of the boundary layer (BL), given by $\boldsymbol{\sigma}^*/(|\boldsymbol{\sigma}^*| + \rho)$, where ρ is some positive constant. Upon replacing the discontinuous function by the BL in the control law of Eq. (15), one obtains:

$$\boldsymbol{v} = -\boldsymbol{B}_{0_\sigma}^{-1}\boldsymbol{A}_{0_\sigma} - \mathbf{G}\frac{\boldsymbol{\sigma}^*}{|\boldsymbol{\sigma}^*| + \rho} - \mathbf{K}\boldsymbol{\sigma}^*. \tag{17}$$

The VSCBL can now avoid chattering, but the invariance principle is not verified any more, theoretically reducing the robustness (such reduction is not significant and the robustness is essentially ensured); however, the smooth control signal is achieved (Martins et al., 2010, 2015). This occurs because the

system dynamics in this case is confined to a neighborhood of the sliding surfaces, and no longer over it, i. e., as a consequence of the approximation with BL the system is enforced to a neighborhood of the manifolds $\boldsymbol{\sigma}(\tilde{\boldsymbol{z}}, t) = 0$ and $\boldsymbol{\sigma}^*(\tilde{\boldsymbol{z}}, t) = 0$, resulting in a reduction of the original robustness, that can still be acceptable. Moreover, realization of the invariance requires that switching between the reaching phase and the sliding phase be ideal, which is impractical. Therefore, the invariance needs an ideal switching, but, in fact, has little practical meaning (Wang and Gao, 1995). Another problem with VSCBL is the need of knowledge of the limits of uncertainties and disturbances in the system, and the application of a large value to the gains $\mathbf{G}$ that can cause a high control effort (large authority control), affecting the trajectory tracking and deteriorating the system performance (Martins et al., 2010).

In order to ensure better results, and not to need the knowledge of the limits of uncertainties and disturbances in the system, in this section a fuzzy logic system is proposed to deal with the chattering.

4.2. Introduction to fuzzy systems

A fuzzy logic system can integrate expert knowledge into the control procedure, without the help of a mathematical model, which makes it feasible in the control of nonlinear systems. Moreover, a fuzzy system can have one or more inputs, and with the help of the expert knowledge, it generates one output.

A fuzzy system has four basic parts, as shown in the block diagram of Fig. 2. Given a set of non-fuzzy entries, from an external system, the fuzzification is responsible for mapping these entries to input fuzzy sets, evaluating the degree of membership of each entry for each fuzzy set. The fuzzy rule base represents the expert knowledge (e.g. provided by a human expert) in the form of linguistic sentences. The rules are written in the form "if ... then ...", describing a definite relation between the input space and the output space. Then, for each rule, the inference machine maps an input set to an output fuzzy set, according to the relation defined by the rules. With this, it combines the fuzzy sets from all the active rules in the rule base into the proper output fuzzy set. Finally, the defuzzification translates fuzzy output to a real number for the system.

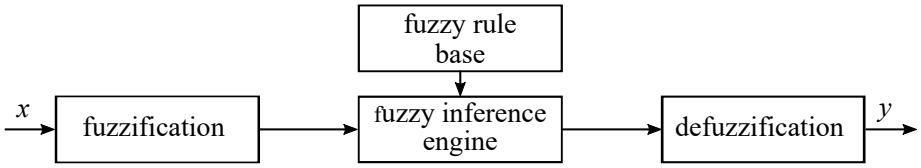

Figure 2. Block diagram representation of a fuzzy system

All the four parts can be mathematically formulated. In this paper, due to the choice of the singleton fuzzification, the center average defuzzification, and the product inference engine, the output of a single input single output (SISO)

fuzzy system can be written as:

$$\boldsymbol{y} = \frac{\sum_{m=1}^{\mathrm{M}} \beta^m \mu^m(x)}{\sum_{m=1}^{\mathrm{M}} \mu^m(x)} = \boldsymbol{\beta}^{\mathrm{T}} \boldsymbol{\psi}(x), \tag{18}$$

where x is the input, y is the output, $\boldsymbol{\beta} = [\beta^1 \ \ldots \ \beta^m \ \ldots \ \beta^{\mathrm{M}}]^{\mathrm{T}}$ is the vector of consequences and $\boldsymbol{\psi}(x) = [\psi^1(x) \ \ldots \ \psi^m(x) \ \ldots \ \psi^{\mathrm{M}}(x)]^{\mathrm{T}}$ is the vector of weights, in which

$$\boldsymbol{\psi}^m(x) = \frac{\mu^m(x)}{\sum_{m=1}^{\mathrm{M}} \mu^m(x)},$$

with μ^m being the membership function of the m rule.

4.3. Design of the adaptive fuzzy variable structure control (AFVSC)

The chattering in the control, presented in Eq. (15), is caused by the constant value of $\mathbf{G}$ and the discontinuous function $sign(\boldsymbol{\sigma}^*)$. Let the control gain $\mathbf{G}sign(\boldsymbol{\sigma}^*)$ be replaced by a fuzzy gain $\hat{\boldsymbol{F}}(\boldsymbol{\sigma}^*)$. The new control input (AFVSC) is then written as:

$$\begin{aligned} \boldsymbol{v} &= -\boldsymbol{B}_{0_\sigma}^{-1} \boldsymbol{A}_{0_\sigma} - \hat{\boldsymbol{F}}(\boldsymbol{\sigma}^*) - \mathbf{K}\boldsymbol{\sigma}^*, \\ &= -\boldsymbol{B}_{0_\sigma}^{-1} \boldsymbol{A}_{0_\sigma} - \hat{\boldsymbol{\beta}}^{\mathrm{T}} \circ \boldsymbol{\psi}(\boldsymbol{\sigma}^*) - \mathbf{K}\boldsymbol{\sigma}^*, \end{aligned} \tag{19}$$

where $\circ$ is a vector element-wise multiplication symbol, the fuzzy control is defined as

$$\hat{\boldsymbol{F}}(\boldsymbol{\sigma}^*) = \hat{\boldsymbol{\beta}}^{\mathrm{T}} \circ \boldsymbol{\psi}(\boldsymbol{\sigma}^*) = [\hat{f}_1(\sigma_1^*) \ \ldots \ \hat{f}_n(\sigma_n^*) \ \ldots \ \hat{f}_{\mathrm{N}}(\sigma_{\mathrm{N}}^*)]^{\mathrm{T}},$$

and each $\hat{f}_n(\sigma_n^*)$ is estimated by an individual fuzzy system that can be written as:

$$\hat{f}_n(\sigma_n^*) = \frac{\sum_{m=1}^{\mathrm{M}} \hat{\boldsymbol{\beta}}_n^m \mu_n^m(\sigma_n^*)}{\sum_{m=1}^{\mathrm{M}} \mu_n^m(\sigma_n^*)} = \hat{\boldsymbol{\beta}}_n^{\mathrm{T}} \boldsymbol{\psi}_n(\sigma_n^*), \tag{20}$$

where $\hat{\boldsymbol{\beta}}_n = [\hat{\beta}_n^1 \ \ldots \ \hat{\beta}_n^m \ \ldots \ \hat{\beta}_n^{\mathrm{M}}]^{\mathrm{T}}$ is the vector of consequences, and the vector of weights is

$$\boldsymbol{\psi}_n(\sigma_n^*) = [\psi_n^1(\sigma_n^*) \ \ldots \ \psi_n^m(\sigma_n^*) \ \ldots \ \psi_n^{\mathrm{M}}(\sigma_n^*)]^{\mathrm{T}}.$$

For the purpose of an online update of the parameters of $\hat{f}_n(\sigma_n^*)$, the consequences $\hat{\boldsymbol{\beta}}_n$ are chosen as the parameters to be updated.

To decide upon the rules for the fuzzy system, consider V as in Eq. (14). V is regarded as an indicator of the energy of $\boldsymbol{\sigma}$. The stability of the system is guaranteed by choosing a control law such that $\dot{V} \leq 0$. In the AFVSC, a fuzzy logic function $\hat{\boldsymbol{F}}(\boldsymbol{\sigma}^*)$ is applied to compensate for the uncertainties and disturbances in the system, and to reduce the energy of $\boldsymbol{\sigma}^*$. In this case, $\dot{V}$ can be rewritten as:

$$\dot{V} = \sum_{n=1}^{\mathrm{N}} \left[\sigma_n^* \left(\tilde{d}_{0_n} - \hat{f}_n(\sigma_n^*)\right)\right] - \boldsymbol{\sigma}^{*^{\mathrm{T}}} \mathbf{K} \boldsymbol{\sigma}^*. \tag{21}$$

Because of the function $sign(\boldsymbol{\sigma}^*)$ the control gain has the same sign as $\boldsymbol{\sigma}^*$. Therefore, $\hat{f}_n(\sigma_n^*)$ should have the same sign as $\boldsymbol{\sigma}_n^*$.

Now, consider $\sigma_n^*[\tilde{d}_{0_n} - \hat{f}_n(\sigma_n^*)]$. When $|\sigma_n^*|$ is large, it is expected that $|\hat{f}_n(\sigma_n^*)|$ is larger so that $\dot{V}$ has a large negative value. This causes the energy of $\boldsymbol{\sigma}^*$ to decay fast. When $|\sigma_n^*|$ is small, $\sigma_n^*[\tilde{d}_{0_n} - \hat{f}_n(\sigma_n^*)]$ is also small and has little effect on the value of $\dot{V}$. Then, $|\hat{f}_n(\sigma_n^*)|$ can be small to avoid chattering. When $|\sigma_n^*|$ is zero, $|\hat{f}_n(\sigma_n^*)|$ is also zero. With this analysis, the rule base is chosen as:

- IF σ_n^* is NB, THEN $\hat{f}_n(\sigma_n^*)$ is $\hat{\beta}_n^1 \psi_n^1(\sigma_n^*)$
- IF σ_n^* is NM, THEN $\hat{f}_n(\sigma_n^*)$ is $\hat{\beta}_n^2 \psi_n^2(\sigma_n^*)$
- IF σ_n^* is NS, THEN $\hat{f}_n(\sigma_n^*)$ is $\hat{\beta}_n^3 \psi_n^3(\sigma_n^*)$
- IF σ_n^* is ZE, THEN $\hat{f}_n(\sigma_n^*)$ is $\hat{\beta}_n^4 \psi_n^4(\sigma_n^*)$
- IF σ_n^* is PS, THEN $\hat{f}_n(\sigma_n^*)$ is $\hat{\beta}_n^5 \psi_n^5(\sigma_n^*)$
- IF σ_n^* is PM, THEN $\hat{f}_n(\sigma_n^*)$ is $\hat{\beta}_n^6 \psi_n^6(\sigma_n^*)$
- IF σ_n^* is PB, THEN $\hat{f}_n(\sigma_n^*)$ is $\hat{\beta}_n^7 \psi_n^7(\sigma_n^*)$

where N stands for negative, P for positive, ZE for zero, S for small, M for medium, and B for big.

The membership functions are chosen to be triangular-shaped functions, as specified in Eq. (22):

$$\mu_n^m(\sigma_n^*) = \begin{cases} 0, & \sigma_n^* \leq \alpha_n^1 \\ \dfrac{\sigma_n^* - \alpha_1}{\alpha_n^2 - \alpha_n^1}, & \alpha_n^1 \leq \sigma_n^* \leq \alpha_n^2 \\ \dfrac{\alpha_n^3 - \sigma_n^*}{\alpha_n^3 - \alpha_n^2}, & \alpha_n^2 \leq \sigma_n^* \leq \alpha_n^3 \\ 0, & \alpha_n^3 \leq \sigma_n^* \end{cases} \tag{22}$$

where α_1 and α_3 determine the "feet" of the triangle and the parameter α_2 locates the peak. The parameters of the input membership functions are predefined and given in Table 1 (see Fig. 3), while those of the output, $\hat{\beta}_n^m$, are updated online, determining the adaptive characteristic of the controller.

Table 1. Parameters of the membership functions of $\boldsymbol{\sigma}^*$

	σ_1^*			σ_2^*		
	α_1^1	α_1^2	α_1^3	α_2^1	α_2^2	α_2^3
NB	$-\infty$	-0.3	-0.2	$-\infty$	-0.5	-0.33
NM	-0.3	-0.2	-0.1	-0.5	-0.33	-0.16
NS	-0.2	-0.1	0	-0.33	-0.16	0
ZE	-0.1	0	0.1	-0.16	0	0.16
PS	0	0.1	0.2	0	0.16	0.33
PM	0.1	0.2	0.3	0.16	0.33	0.5
PB	0.2	0.3	∞	0.33	0.5	∞

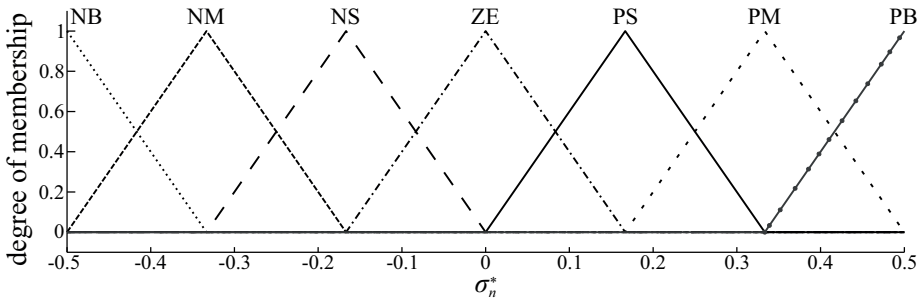

Figure 3. Triangular-shaped input membership functions

It must be emphasized that the processing time required when using fuzzy logic control depends upon the number of rules that must be evaluated. Therefore, large systems with many rules would require very powerful and fast processors to compute in real time. The smaller the rule base, the less computational power needed (Mishra, 2014). Thus, unlike a pure fuzzy logic controller, which is encountered in the rule expanding problem, the AFVSC uses only 7 if-then rules in the rule base with respect to sliding surfaces, and it also uses triangular membership functions, making their structure even simpler. Therefore, it is more suitable for implementation in the real DWMRs compared to the proposals forwarded in Xie et al. (2012), Keighobadi and Mohamadi (2011a,b), Keighobadi and Menhaj (2012), or Mishra (2014). In addition, the reasons to choose this fuzzy inference system against the background of other methods are: simplicity of the model and efficient control of the system, due to being best suited for control applications. It is used often due to the intuitive nature of the system and ease in designing. Further details, concerning this choice can be found in Chaudhari and Patil (2014a,b).

4.4. Stability analysis of the AFVSC

Since $\hat{\beta}_n$ is chosen as the parameter of $\hat{f}_n(\sigma_n^*)$ to be online updated, we define $\boldsymbol{\beta}_n$ so that $f_n(\sigma_n^*) = \boldsymbol{\beta}_n^{\mathrm{T}}\boldsymbol{\psi}_n(\sigma_n)$ is the optimal compensation for $\tilde{d}_{0_n}$. According to Wang's theorem (Wang, 1999; Guo and Woo, 2003; Li et al., 2004) there exists $\gamma_n > 0$, satisfying

$$|\tilde{d}_{0_n} - \boldsymbol{\beta}_n^{\mathrm{T}}\boldsymbol{\psi}_n(\sigma_n^*)| \leq \gamma_n, \qquad \tilde{\boldsymbol{d}}_0 = \Delta\boldsymbol{f}, \tag{23}$$

where γ_n can be as small as possible, i.e., $0 < \gamma_n < 1$. Now, define the estimation error as

$$\tilde{\boldsymbol{\beta}}_n = \hat{\boldsymbol{\beta}}_n - \boldsymbol{\beta}_n, \tag{24}$$

so that Eq. (20) can be rewritten as:

$$\hat{f}_n(\sigma_n^*) = \tilde{\boldsymbol{\beta}}_n^{\mathrm{T}}\boldsymbol{\psi}_n(\sigma_n^*) + \boldsymbol{\beta}_n^{\mathrm{T}}\boldsymbol{\psi}_n(\sigma_n^*). \tag{25}$$

From Eq. (24) and Eq. (25) the following adaptive law can be derived:

$$\dot{\tilde{\boldsymbol{\beta}}}_n = \dot{\hat{\boldsymbol{\beta}}}_n = \boldsymbol{\sigma}_n^*\boldsymbol{\psi}_n(\sigma_n^*). \tag{26}$$

From the adaptation law, given in Eq. (26), the stability analysis of the AFVSC could be done starting from the following Lyapunov function candidate:

$$V = \frac{1}{2}\left[\boldsymbol{\sigma}^{\mathrm{T}}\boldsymbol{\sigma} + \sum_{n=1}^{\mathrm{N}}\left(\tilde{\boldsymbol{\beta}}_n^{\mathrm{T}}\tilde{\boldsymbol{\beta}}_n\right)\right] \tag{27}$$

where $\tilde{\boldsymbol{\beta}}_n^{\mathrm{T}}\tilde{\boldsymbol{\beta}}_n > 0$, so that V is positive definite. By differentiating Eq. (27), one obtains:

$$\begin{aligned}
\dot{V} &= \boldsymbol{\sigma}^{\mathrm{T}}\dot{\boldsymbol{\sigma}} + \sum_{n=1}^{\mathrm{N}}\tilde{\boldsymbol{\beta}}_n^{\mathrm{T}}\dot{\tilde{\boldsymbol{\beta}}}_n \\
&= \boldsymbol{\sigma}^{\mathrm{T}}\boldsymbol{A}_{0_\sigma} + \boldsymbol{\sigma}^{\mathrm{T}}\boldsymbol{B}_{0_\sigma}\boldsymbol{v} + \boldsymbol{\sigma}^{\mathrm{T}}\boldsymbol{d}_\sigma + \sum_{n=1}^{\mathrm{N}}\tilde{\boldsymbol{\beta}}_n^{\mathrm{T}}\dot{\tilde{\boldsymbol{\beta}}}_n \\
&= \boldsymbol{\sigma}^{\mathrm{T}}\boldsymbol{B}_{0_\sigma}\boldsymbol{B}_{0_\sigma}^{-1}\boldsymbol{A}_{0_\sigma} + \boldsymbol{\sigma}^{\mathrm{T}}\boldsymbol{B}_{0_\sigma}\boldsymbol{v} + \boldsymbol{\sigma}^{\mathrm{T}}\boldsymbol{B}_{0_\sigma}\tilde{\boldsymbol{d}}_0 + \sum_{n=1}^{\mathrm{N}}\tilde{\boldsymbol{\beta}}_n^{\mathrm{T}}\dot{\tilde{\boldsymbol{\beta}}}_n \\
&= \left(\boldsymbol{B}_{0_\sigma}^{\mathrm{T}}\boldsymbol{\sigma}\right)^{\mathrm{T}}\boldsymbol{B}_{0_\sigma}^{-1}\boldsymbol{A}_{0_\sigma} + \left(\boldsymbol{B}_{0_\sigma}^{\mathrm{T}}\boldsymbol{\sigma}\right)^{\mathrm{T}}\left(\boldsymbol{v} + \tilde{\boldsymbol{d}}_0\right) + \sum_{n=1}^{\mathrm{N}}\tilde{\boldsymbol{\beta}}_n^{\mathrm{T}}\dot{\tilde{\boldsymbol{\beta}}}_n \\
&= \boldsymbol{\sigma}^{*^{\mathrm{T}}}\boldsymbol{B}_{0_\sigma}^{-1}\boldsymbol{A}_{0_\sigma} + \boldsymbol{\sigma}^{*^{\mathrm{T}}}\left(\boldsymbol{v} + \tilde{\boldsymbol{d}}_0\right) + \sum_{n=1}^{\mathrm{N}}\tilde{\boldsymbol{\beta}}_n^{\mathrm{T}}\dot{\tilde{\boldsymbol{\beta}}}_n.
\end{aligned}$$

Using the control law from Eq. (19) (AFVSC), and replacing Eq. (23) and Eq. (25), we obtain for $\dot{V}$:

$$\begin{aligned}
\dot{V} &= \boldsymbol{\sigma^*}^{\mathrm{T}} \boldsymbol{B}_{0_\sigma}^{-1} \boldsymbol{A}_{0_\sigma} - \boldsymbol{\sigma^*}^{\mathrm{T}} \boldsymbol{B}_{0_\sigma}^{-1} \boldsymbol{A}_{0_\sigma} - \boldsymbol{\sigma^*}^{\mathrm{T}} \hat{\boldsymbol{F}}(\boldsymbol{\sigma^*}) - \boldsymbol{\sigma^*}^{\mathrm{T}} \mathbf{K} \boldsymbol{\sigma^*} + \boldsymbol{\sigma^*} \tilde{\boldsymbol{d}}_0 + \sum_{n=1}^{\mathrm{N}} \tilde{\boldsymbol{\beta}}_n^{\mathrm{T}} \dot{\hat{\boldsymbol{\beta}}}_n \\
&= -\boldsymbol{\sigma^*}^{\mathrm{T}} \left[\tilde{\boldsymbol{\beta}}^{\mathrm{T}} \circ \boldsymbol{\psi}(\boldsymbol{\sigma^*}) \right] - \boldsymbol{\sigma^*}^{\mathrm{T}} \left[\boldsymbol{\beta}^{\mathrm{T}} \circ \boldsymbol{\psi}(\boldsymbol{\sigma^*}) \right] - \boldsymbol{\sigma^*}^{\mathrm{T}} \mathbf{K} \boldsymbol{\sigma^*} + \boldsymbol{\sigma^*}^{\mathrm{T}} \Delta \boldsymbol{f} + \sum_{n=1}^{\mathrm{N}} \tilde{\boldsymbol{\beta}}_n^{\mathrm{T}} \dot{\hat{\boldsymbol{\beta}}}_n \\
&= \sum_{n=1}^{\mathrm{N}} \sigma_n^* \left[\Delta f_n - \left(\tilde{\boldsymbol{\beta}}_n^{\mathrm{T}} \boldsymbol{\psi}_n(\sigma_n^*) + \boldsymbol{\beta}_n^{\mathrm{T}} \boldsymbol{\psi}_n(\sigma_n^*) \right) \right] - \boldsymbol{\sigma^*}^{\mathrm{T}} \mathbf{K} \boldsymbol{\sigma^*} + \sum_{n=1}^{\mathrm{N}} \tilde{\boldsymbol{\beta}}_n^{\mathrm{T}} \dot{\hat{\boldsymbol{\beta}}}_n \\
&= -\boldsymbol{\sigma^*}^{\mathrm{T}} \mathbf{K} \boldsymbol{\sigma^*} + \sum_{n=1}^{\mathrm{N}} \sigma_n^* \left[\Delta f_n - \boldsymbol{\beta}_n^{\mathrm{T}} \boldsymbol{\psi}_n(\sigma_n^*) \right] - \sum_{n=1}^{\mathrm{N}} \sigma_n^* \tilde{\boldsymbol{\beta}}_n^{\mathrm{T}} \boldsymbol{\psi}_n(\sigma_n^*) + \sum_{n=1}^{\mathrm{N}} \tilde{\boldsymbol{\beta}}_n^{\mathrm{T}} \dot{\hat{\boldsymbol{\beta}}}_n \\
&= -\boldsymbol{\sigma^*}^{\mathrm{T}} \mathbf{K} \boldsymbol{\sigma^*} + \sum_{n=1}^{\mathrm{N}} \sigma_n^* \left[\Delta f_n - \boldsymbol{\beta}_n^{\mathrm{T}} \boldsymbol{\psi}_n(\sigma_n^*) \right] + \sum_{n=1}^{\mathrm{N}} \tilde{\boldsymbol{\beta}}_n^{\mathrm{T}} \left(-\sigma_n^* \boldsymbol{\psi}_n(\sigma_n^*) + \dot{\hat{\boldsymbol{\beta}}}_n \right),
\end{aligned}$$

while by replacing the adaptive law, Eq. (26), $\dot{V}$ yields:

$$\begin{aligned}
\dot{V} &= -\boldsymbol{\sigma^*}^{\mathrm{T}} \mathbf{K} \boldsymbol{\sigma^*} + \sum_{n=1}^{\mathrm{N}} \sigma_n^* \left[\Delta f_n - \boldsymbol{\beta}_n^{\mathrm{T}} \boldsymbol{\psi}_n(\sigma_n^*) \right] + \sum_{n=1}^{\mathrm{N}} \tilde{\boldsymbol{\beta}}_n^{\mathrm{T}} \left(-\sigma_n^* \boldsymbol{\psi}_n(\sigma_n^*) + \sigma_n^* \boldsymbol{\psi}_n(\sigma_n^*) \right) \\
&= -\boldsymbol{\sigma^*}^{\mathrm{T}} \mathbf{K} \boldsymbol{\sigma^*} + \sum_{n=1}^{\mathrm{N}} \sigma_n^* \left[\Delta f_n - \boldsymbol{\beta}_n^{\mathrm{T}} \boldsymbol{\psi}_n(\sigma_n^*) \right].
\end{aligned} \tag{28}$$

From Eq. (23), assume that:

$$|\Delta f_n - \boldsymbol{\beta}_n^{\mathrm{T}} \boldsymbol{\psi}_n(\sigma_n^*)| \leq \gamma_n \leq \phi_n |\sigma_n^*|,$$

where $0 < \phi_n < 1$. Then, the second term at the right hand side of Eq. (28) satisfies

$$\sigma_n^* |\Delta f_n - \boldsymbol{\beta}_n^{\mathrm{T}} \boldsymbol{\psi}_n(\sigma_n^*)| \leq \phi_n |\sigma_n^*|^2 = \phi_n {\sigma_n^*}^2,$$

and therefore

$$\dot{V} \leq -\boldsymbol{\sigma^*}^{\mathrm{T}} \mathbf{K} \boldsymbol{\sigma^*} + \sum_{n=1}^{\mathrm{N}} \phi_n {\sigma_n^*}^2. \tag{29}$$

The right hand side of Eq. (29) can now be written as

$$\dot{V} \leq \sum_{n=1}^{\mathrm{N}} (-\kappa_n {\sigma_n^*}^2 + \phi_n {\sigma_n^*}^2) = -\boldsymbol{\sigma^*}^{\mathrm{T}} (\mathbf{K} - \boldsymbol{\Phi}) \boldsymbol{\sigma^*} \leq 0.$$

where $\mathbf{K} = diag[\kappa_1 \ \ldots \ \kappa_n \ \ldots \ \kappa_{\mathrm{N}}]$ and $\mathbf{\Phi} = diag[\phi_1 \ \ldots \ \phi_n \ \ldots \ \phi_{\mathrm{N}}]$. Simply choose $\kappa_n > \phi_n$, so that $(\mathbf{K} - \mathbf{\Phi})$ is a positive definite matrix, and therefore $\dot{V} \leq 0$. Since $(\mathbf{K} - \mathbf{\Phi})$ is a positive definite matrix, $\dot{V} = 0$ only when $\boldsymbol{\sigma}^* = 0$. Thus, the AFVSC is asymptotically stable.

5. Simulations results and RT implementations

5.1. The setup

In order to verify the performance of the controllers described in Sections 3 and 4, the VSCBL and the AFVSC are implemented in Matlab/Simulink software, version R2014a, and evaluated for the trajectory tracking control problem by means of simulation using MobileSim simulator, and experiments in the Power-Bot DWMR itself. The Matlab/Simulink executions were performed with the Euler solver for equation integration with sampling time of 5 ms. Other integration methods were tested, but only with at most marginal improvement.

An eight-shaped trajectory (Oriolo, De Luca and Venditelli, 2002) was used as reference. The mathematical formulation of the trajectory is given by Eqs. (30):

$$\begin{aligned} \boldsymbol{v}_{\mathrm{r}} &= \begin{bmatrix} \nu_{\mathrm{r}} \\ \omega_{\mathrm{r}} \end{bmatrix} = \begin{bmatrix} \sqrt{\dot{x}_{\mathrm{r}}^2 + \dot{y}_{\mathrm{r}}^2} \\ \dot{\theta}_{\mathrm{r}} \end{bmatrix}, \\ \dot{\boldsymbol{q}}_{\mathrm{r}} &= \begin{bmatrix} \dot{x}_{\mathrm{r}} \\ \dot{y}_{\mathrm{r}} \\ \dot{\theta}_{\mathrm{r}} \end{bmatrix} = \begin{bmatrix} \dfrac{3\pi}{50} \sin\left(\dfrac{\pi}{25}t + \dfrac{\pi}{2}\right) \\ -\dfrac{3\pi}{25} \cos\left(\dfrac{\pi}{25}t + \dfrac{\pi}{2}\right) \\ \dfrac{\ddot{y}_{\mathrm{r}}\dot{x}_{\mathrm{r}} - \ddot{x}_{\mathrm{r}}\dot{y}_{\mathrm{r}}}{\dot{x}_{\mathrm{r}}^2 + \dot{y}_{\mathrm{r}}^2} \end{bmatrix}. \end{aligned} \tag{30}$$

In the trajectory, the DWMR starts with an initial error of $\boldsymbol{q}_{\mathrm{e}} = [0.15 \ 0.2 \ \frac{\pi}{6}]^{\mathrm{T}}$. The gains of the sliding surfaces are $\Lambda_1 = 1.5$, $\Lambda_2 = 6.0$ and $\Lambda_3 = 1.0$, and the gains of the kinematic and dynamic controllers are presented in Table 2.

Table 2. Gains of the kinematic and dynamic controllers

Gain	Controller	
	VSCBL	AFVSC
g_1	0.1	-
g_2	0.3	-
κ_1	0.1	0.1
κ_2	0.1	0.1
ρ	0.1	-
$\mathrm{k}_{\mathrm{p}_\nu}$	40.0	40.0
$\mathrm{k}_{\mathrm{p}_\omega}$	40.0	40.0
$\mathrm{k}_{\mathrm{d}_\nu}$	20.0	20.0
$\mathrm{k}_{\mathrm{d}_\omega}$	20.0	20.0

Unfortunately, the PowerBot DWMR is closed and there is an internal PID controller that tracks these inputs with a sampling time of 5 ms. Thus, only the PD controller can be considered as dynamic controller for simulations in the MobileSim simulator, and experiments in the PowerBot DWMR itself. Actually, this unpleasant situation is commonly found in the literature of robotics, like in Spong, Hutchinson and Vidjasagar (2006) or in Elyoussef et al. (2014). Although it is not possible to implement a direct torque controller, sufficient analysis results are obtained by studying two different control structures, comprising the PD controller integrated with the following kinematic controllers: VSCBL and AFVSC.

5.2. Simulation results in the realistic scenario

The first simulation scenario, called the realistic scenario, instead of using the kinematics, Eq. (1), and dynamics, Eq. (2), developed in Section 2 to represent the behavior of the DWMR, used the MobileSim simulator.

MobileSim is a software designed to simulate the behavior of MobileRobots platforms produced by Mobile Robots Inc. for debugging and experimentation. To establish communication between the controller in Matlab/Simulink, and the MobileSim simulator, ARIA is used. ARIA (Advanced Robot Interface for Applications) is a library for all MobileRobots platforms, capable of dynamically controlling the DWMRs velocity, heading, relative heading, and other motion parameters. ARIA also receives position estimation, sonar readings, and all other current operating data sent by the robotic platform.

The block diagram, presented in Fig. 4, shows how ARIA and MobileSim simulator were used to perform the simulations in the realistic scenario. The blocks of Fig. 4 have the following meaning: the Reference Trajectory block generates the reference posture $\boldsymbol{q}_{\mathrm{r}}$ and reference velocity $\boldsymbol{v}_{\mathrm{r}}$. With the reference posture, and the real posture $\boldsymbol{q}$ of the DWMR, the Sum block calculates the posture error $\boldsymbol{q}_{\mathrm{e}}$, as in Eq. (7). The Kinematic Controller block, with the posture error and the reference velocity, calculates the control velocities $\boldsymbol{v}_{\mathrm{c}}$ using the control law of Eq. (17) with respect to the VSCBL, as well as Eq. (19) and Eq. (26) with respect to the AFVSC. The velocity, calculated by the controller, passes to the ARIA Function block. This block establishes the communication between Matlab/Simulink and the MobileSim simulator. The MobileSim block simulates the DWMR behavior, and gives the real posture $\boldsymbol{q}$ of the DWMR. Again, an ARIA Function block is needed to receive the posture information from the MobileSim simulator, which is used to calculate the posture error.

VSCBL and the AFVSC were simulated in the realistic scenario for the eight-shaped trajectory. This trajectory was selected because it features deceleration and acceleration, together with the assumed initial error. The simulation results of the trajectory tracking include: posture tracking and orientation errors, control velocities, reference velocities and velocities of the DWMR, sliding surfaces and new sliding surfaces, auxiliary velocity tracking errors and compensations of the VSCBL and AFVSC.

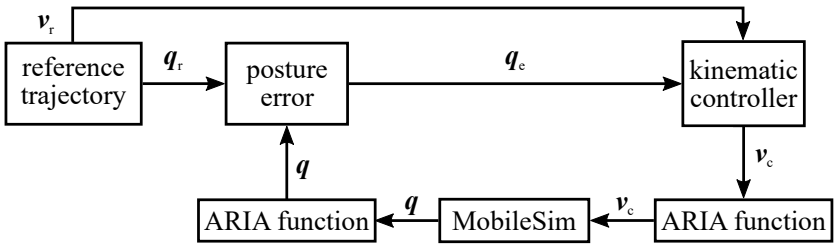

Figure 4. Block diagram of the simulations in the realistic scenario

The results, presented in Table 3, containing RMS of the errors, show that the controllers can track the trajectories with minimum error even with uncertainties and disturbances (e.g., external disturbances) provided by the MobileSim simulator.

Table 3. RMS of the errors - simulation results for the realistic scenario using MobileSim simulator

Controller	RMS error	Eight-shaped trajectory
VSCBL	xy_e	0.1279
	θ_e	0.0982
AFVSC	xy_e	0.1252
	θ_e	0.0940

The reference trajectory, with respect to the trajectory realized by the DWMR using the controllers, is illustrated in Fig. 5. From this figure, it can be established that both controllers lead the DMWR to reach the trajectory at a similar point and that it remains near the trajectory during the remaining time, i.e., the DWMR tracks the reference trajectory.

Figure 6 shows the posture tracking and orientation errors. The tracking error of the VSCBL varies slightly more than that of the AFVSC. But for both, the errors tend to zero with a slight variation of the orientation error when the DWMR makes a curve. (Note, please, that all figures, starting with Fig. 6, have been placed at the end of the paper.)

In Fig. 7, the control velocities are presented. The VSCBL and the AFVSC show smooth control signals. This behavior can also be observed in Fig. 8, in which the velocities of the DWMR track the reference.

For the use of the VSCBL and AFVSC, the sliding surfaces and the new sliding surfaces tend to converge to zero, as can be seen in Figs. 9 and 10, without chattering phenomenon.

The auxiliary velocity tracking errors $\boldsymbol{v}_e$, seen as disturbances for the kinematic model, and given by the difference between the control velocities $\boldsymbol{v}_c$ and the real velocities of the DWMR $\boldsymbol{v}$, appear because of uncertainties and disturbances (e.g., parametric variations, unmodeled dynamics and physical lim-

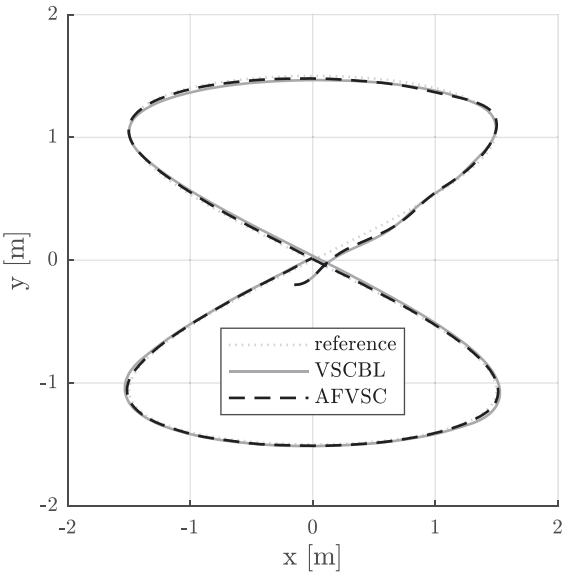

Figure 5. Trajectory tracking in the realistic scenario

itations). Figures 11 and 12 show the auxiliary velocity tracking errors and compensations for each controller.

For this scenario, Figs. 7 and 8 show how the DWMR cannot switch instantaneously the control velocities and the velocities of the DWMR, generating large auxiliary velocity tracking errors. As a consequence, regarding both the VSCBL and the AFVSC, Figs. 11 and 12 present auxiliary velocity tracking errors and compensations, whose magnitudes show opposite behaviors in absolute terms, having the aim of cancelling the auxiliary velocity tracking errors. The compensations tend to converge to zero.

The AFVSC presents slightly better tracking results than the VSCBL, and the clear advantage of the AFVSC is also that it does not require the *a priori* knowledge of the boundaries of the uncertainties and disturbances (e.g., external disturbances). On the other hand, the VSCBL requires such knowledge in order to define the gain values $\mathbf{G}$ to achieve a satisfactory tracking performance, without unnecessary control efforts regarding the actuators of the DWMR.

5.3. Implementations in real time

After the simulations in the realistic scenario, the proposed controller was tested using the Powerbot DWMR. Powerbot DWMR is a high-payload differential drive robotic platform for research and rapid prototyping. It is an ideal platform for laboratory and research tasks, involving delivery, navigation and ma-

nipulation. It is an automated guided vehicle, specially designed and equipped for autonomous, intelligent delivery and handling of large payloads. Powerbot DWMR is a member of MobileRobots Pioneer family of mobile robots, which are research and development platforms that share a common architecture, foundation software and employ intelligence based client-server robotics control (see Filipescu et al., 2011). Table 4 shows the parameters of the Powerbot DWMR.

Table 4. Parameter specifications of the Powerbot DWMR

Parameter	Value
Mass of the DWMR body	120 kg
Maximum payload	100 kg
Radius of the drive wheel	0.135 m
DWMR length	0.9 m
DWMR width	0.66 m
DWMR height	0.48 m
Moment of inertia	15.0656 kg.m^2
Maximum linear velocity	2.1 m/s
Maximum angular velocity	$\frac{5\pi}{3}$ rad/s $\approx$ 5.24 rad/s
Maximum torque in DC motor	20.45 Nm

Figure 13 shows the block diagram of the experiment execution as the simulator MobileSim is replaced by the Powerbot DWMR. ARIA is still used for the communication between the Matlab/Simulink and the Powerbot DWMR. This communication is carried out by a serial port.

Finally, the VSCBL and the AFVSC were tested in the Powerbot DWMR for the eight-shaped trajectory. Table 5 presents the RMS of the errors for this experiment.

Table 5. RMS of the errors - experimental results

Controllers	RMS errors	Eight-shaped trajectory
VSCBL	xy_{e}	0.0894
	θ_{e}	0.1180
AFVSC	xy_{e}	0.0892
	θ_{e}	0.1176

The experimental results in real time, presented in Table 5, confirm what was observed in the simulation results, namely that both VSCBL and AFVSC can track the trajectory with minimum errors. Figures 14 to 21 show graphically the experimental results of the VSCBL and AFVSC on the Powerbot DWMR.

For the controllers, Fig. 14 shows how the DWMR reaches the reference trajectory, and remains on it for the subsequent time.

In Fig. 15, by using VSCBL and AFVSC, it is observed how the posture tracking and orientation errors tend to zero and stay there for the remainder of

the experiment. The variation of the orientation error has a behavior similar to that obtained in the MobileSim simulator (realistic scenario).

The control velocities, generated by the VSCBL and AFVSC have smooth control signals, as illustrated in Fig. 16. With respect to the velocities of DWMR, it can be observed in Fig. 17 that these velocities track the reference velocities.

From the observation of Figs. 18 and 19, it can be seen that the sliding surfaces and the new sliding surfaces tend to converge to zero and are free from chattering, for both the VSCBL and AFVSC.

Figures 20 and 21 show that the controllers are robust with respect to matched uncertainties and disturbances, with behaviors of auxiliary velocity tracking errors and compensations being similar to behaviors obtained in the MobileSim simulator (realistic scenario).

In short, the results in the experimental scenario are are in agreement with the results obtained in the simulated realistic scenario.

Based on the experimental results, it was demonstrated that Remark 2.1, provided in Wang and Gao (1995) is true, i.e., that the realization of the invariance requires that switching between the reaching phase and the sliding phase be ideal, which is impractical. Therefore, the invariance is ideal, but this has little practical meaning.

6. Conclusions

In this paper, the integration of a kinematic controller (AFVSC) and dynamic controller (PD control) as a solution to the trajectory tracking problem applied to DWMRs, was proposed. For purposes of performance comparison with the AFVSC, the kinematic controller, a VSCBL, was also integrated with the PD controller, demonstrating that the incidence of uncertainties and disturbances produces auxiliary velocity tracking errors. The results obtained in simulated realistic and experimental scenarios have shown that: the AFVSC has better performance than the VSCBL, indicating that the invariance has little practical meaning, the robustness is ensured and a smooth control signal is achieved; the advantages of the AFVSC in comparison to the VSCBL were verified, making it more suitable for implementation in real wheeled mobile robots when compared to the related proposals from the literature; the stability analysis of the closed-loop control system with the adaptation law of the fuzzy system was successfully performed using Lyapunov theory.

In future works, it is envisaged to carry out the comparison of AFVSC with other existing chattering reduction approaches (including other fuzzy controllers) and to use the AFVSC in the DWMR group formation control problem.

7. Acknowledgments

The authors would like to acknowledge the CAPES for the financial support.

References

BEGNINI, M., BERTOL, D. W. and MARTINS, N. A. (2017)A robust adaptive fuzzy variable structure tracking control for the wheeled mobile robot: simulation and experimental results. *Control Engineering Practice* 64, 27–43.

CHAUDHARI, S.R. and PATIL, M.E. (2014) A comparative analysis of fuzzy inference systems for air conditioner. *International Journal of Advanced Computer Research*, **4**, 4, 922–927.

CHAUDHARI, S.R. and PATIL, M.E. (2014) Study and review of fuzzy inference systems for decision making and control. *American International Journal of Research Science, Technology, Engineeringand Mathematics*, **5**, 88–92.

ELYOUSSEF, E.S., MARTINS, N.A., DE PIERI, E.R. and MORENO, U.F. (2014) Pd-super-twisting second order sliding mode tracking control for a nonholonomic wheeled mobile robot. In: *Proceedings of the 19th World Congress of the International Federation of Automatic Control (IFAC World Congress)*, **11**, 3827–3832.

ERBATUR, K. and KAYNAK, O. (2001) Use of adaptive fuzzy systems in parameter tuning of sliding-mode controllers. *IEEE/ASME Trans. Mechatronics*, **6**, 4, 474–482.

FARRELL, J.A. and POLYCARPOU, M.M. (2006) *Adaptive Approximation Based Control: Unifying Neural, Fuzzy and Traditional Adaptive Approximation Approaches.* 1st edition, John Wiley & Sons, Inc., Wiley-Interscience.

FIERRO, R. and LEWIS, F.L. (1998) Control of a nonholonomic mobile robot using neural networks. *IEEE Transactions on Neural Networks*, **9**, 4, 589–600.

FILIPESCU, A., MINZU, V., DUMITRASCU, B. and MINCA, E. (2011) Trajectory tracking and discrete-time sliding-mode control of wheeled mobile robots. In: *Proceedings of the 2011 IEEE International Conference on Information and Automation (ICIA 2011).* IEEE, 27–32.

GUO, Y. and WOO, P.Y. (2003) An adaptive fuzzy sliding mode controller for robotic manipulators. *IEEE Transactions on Systems, Man and Cybernetics, Part A: Systems and Humans*, **33**, 2, 149–159.

KANAYAMA, Y., KIMURA, Y., MIYAZAKI, F. and NOGUCHI, T. (1991) A stable tracking control method for a non-holonomic mobile robot. In: *Proceedings of the IEEE/RSJ International Workshop on Intelligent Robots and Systems (IROS'1991).* IEEE, 1236–1241.

KAYNAK, O., ERBATUR, K. and ERTUGNRL, M. (2001) The fusion of computationally intelligent methodologies and sliding mode control - a survey. *IEEE Transactions on Industrial Electronics*, **48**, 1, 4–17.

KEIGHOBADI, J. and MENHAJ, M.B. (2012) From nonlinear to fuzzy approaches in trajectory tracking control of wheeled mobile robots. *Asian Journal of Control*, **14**, 4, 960–973.

KEIGHOBADI, J. and MOHAMADI, Y. (2011a) Fuzzy sliding mode control of a nonholonomic wheeled mobile robot. In: *Proceedings of the 2011 International MultiConference of Engineers and Computer Scientists (IMECS '2011)*. 2, 1–6.

KEIGHOBADI, J. and MOHAMADI, Y. (2011b) Fuzzy sliding mode control of nonholonomic wheeled mobile robot. In: *Proceedings of the 2011 IEEE 9th International Symposium on Applied Machine Intelligence and Informatics (SAMI'2011)*. IEEE, 273–278.

KUNG, C.C. and CHEN, T.H. and KUNG, L.-H. (2005) Modified adaptive fuzzy sliding mode controller for uncertain nonlinear systems. *IEICE Trans. Fundamentals*, **E88-A**, 5, 1328–1334.

KUNG, C.C. and CHEN, T.H. (2007) Hoo tracking-based adaptive fuzzy sliding mode controller design for nonlinear systems. *IET Control Theory & Applications*, **1**, 1, 82–89.

LEE, J.H., LIN, C., LIM, H. and LEE, J.M. (2009) Sliding mode control for trajectory tracking of mobile robot in the rfid sensor space. *International Journal of Control. Automation and Systems*, **7**, 3, 429–435.

LI, Y., QIANG, S., ZHUANG, X. and KAYNAK, O. (2004) Robust and adaptive backstepping control for nonlinear systems using rbf neural networks. *IEEE Transactions on Neural Networks*, **15**, 3, 693–701.

MARTINS, N.A., ALENCAR, M., LOMBARDI, W.C., BERTOL, D.W., DE PIERI, E.R. and FERASOLI FILHO, H. (2015) Trajectory tracking of a wheeled mobile robot with uncertainties and disturbances: proposed adaptive neural control. *Control and Cybernetics*, **44**, 1, 47–98.

MARTINS, N.A., ELYOUSSEF, E.S., BERTOL, D.W., DE PIERI, E.R., MORENO, U.F. and CASTELAN, E.B. (2010) Nonholonomic mobile robot with kinematic disturbances in the trajectory tracking: a variable structure controller. *Learning and Nonlinear Models*, **8**, 1, 23–40.

MISHRA, E.A. (2014) Trajectory tracking of differential drive wheeled mobile robot. *International Journal on Mechanical Engineering and Robotics (IJMER'2014)*, **2**, 2, 28–31.

ORIOLO, G., DE LUCA, A. and VENDITTELLI, M. (2002) WMR control via dynamic feedback linearization: design, implementation, and experimental validation. *IEEE Transactions on Control Systems Technology*, **10**, 6, 835–852.

PARK, B.S., YOO, S.J., PARK, J.B. and CHOI, Y.H. (2009) Adaptive neural sliding mode control of nonholonomic wheeled mobile robots with model uncertainty. *IEEE Transactions on Control Systems Technology*, **17**, 1, 207–214.

SPONG, M.W., HUTCHINSON, S. and VIDYASAGAR, M. (2006) *Robot Modeling and Control*. Wiley, New York.

UTKIN, V.I. (1993) Sliding mode control design: Principles and applications to electric drives. *IEEE Trans. Industrial Electronics*, **40**, 1, 23–36.

UTKIN, V.I., GULDNER, J. and SHI, J. (2009) *Sliding Mode Control in Electromechanical Systems*, **34**. CRC Press.

WAI, R.J. (2007) Fuzzy sliding-mode control using adaptive tuning technique. *IEEE Trans. Industrial Electronics*, **54**, l, 586–594.

WANG, L.X. (1999) *A Course in Fuzzy Systems and Control*. Prentice-Hall Press, Englewood Cliffs, USA.

WANG, S. and GAO, W. (1995) Robustness and invariance of variable structure systems with multiple inputs. In: *Proceedings of the American Control Conference (ACC'1995)*. IEEE, 1, 1035–1039.

XIE, M.J., LI, L.T. and WANG, Z.Q. (2012) Robust adaptive control of a wheeled mobile robot violating the pure nonholonomic constraint. In: *Proceedings of the 10th World Congress on Intelligent Control and Automation (WCICA'2012)*. IEEE, 2706–2709.

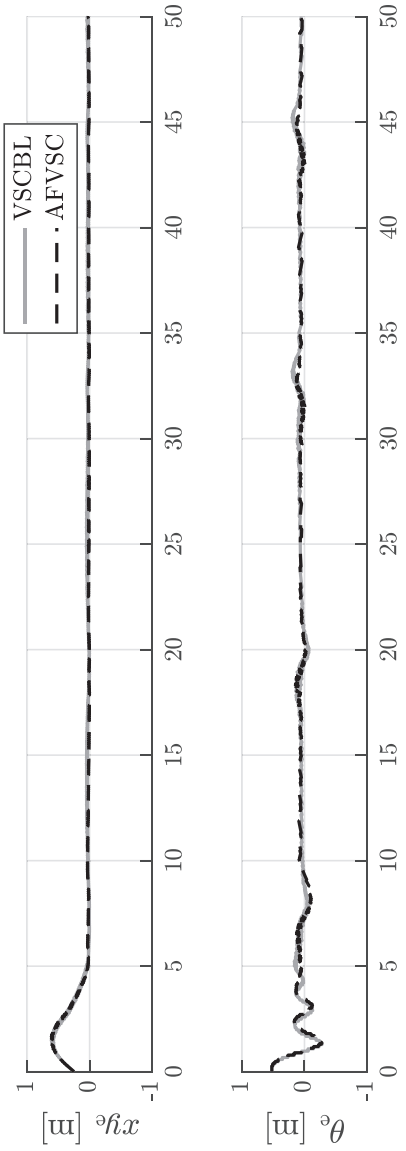

Figure 6. Posture tracking and orientation errors in the realistic scenario

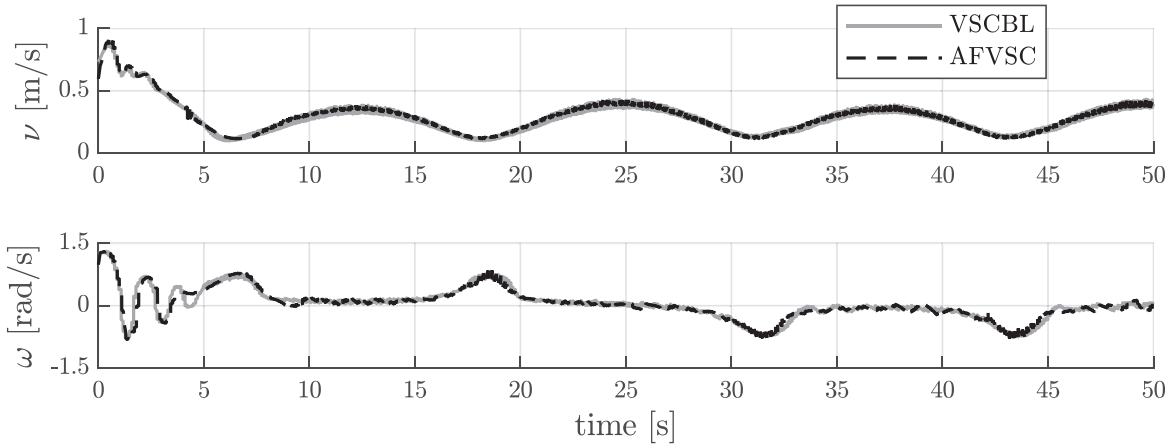

Figure 7. Control velocities in the realistic scenario

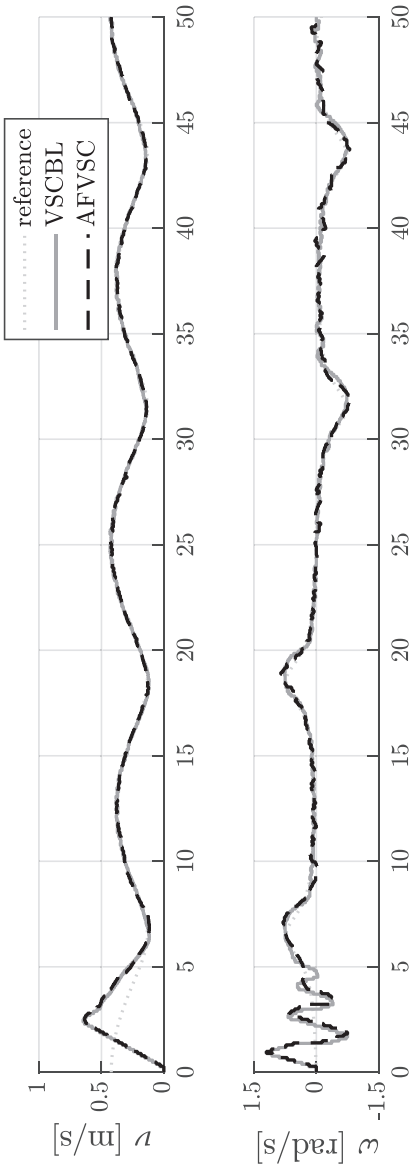

Figure 8. Velocities of the DWMR and reference velocities in the realistic scenario

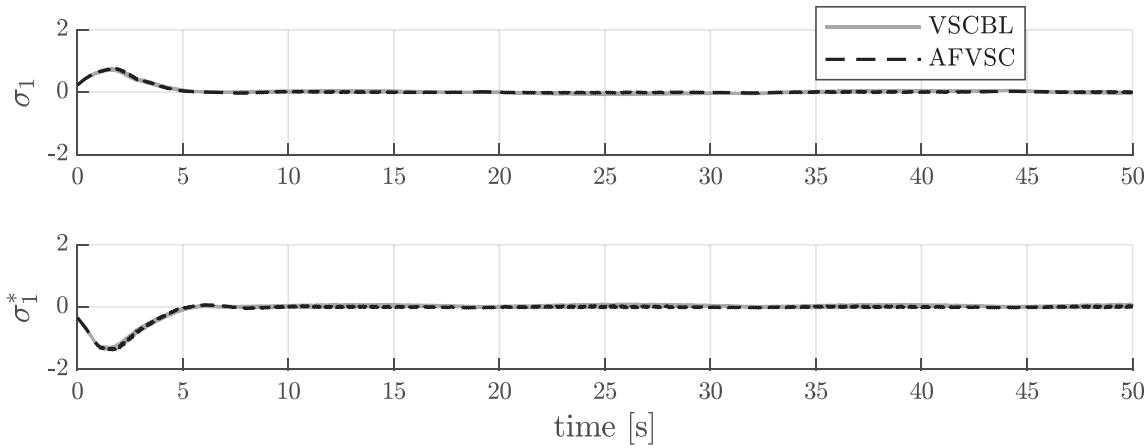

Figure 9. Sliding surface σ_1 and new sliding surface σ_1^* in the realistic scenario

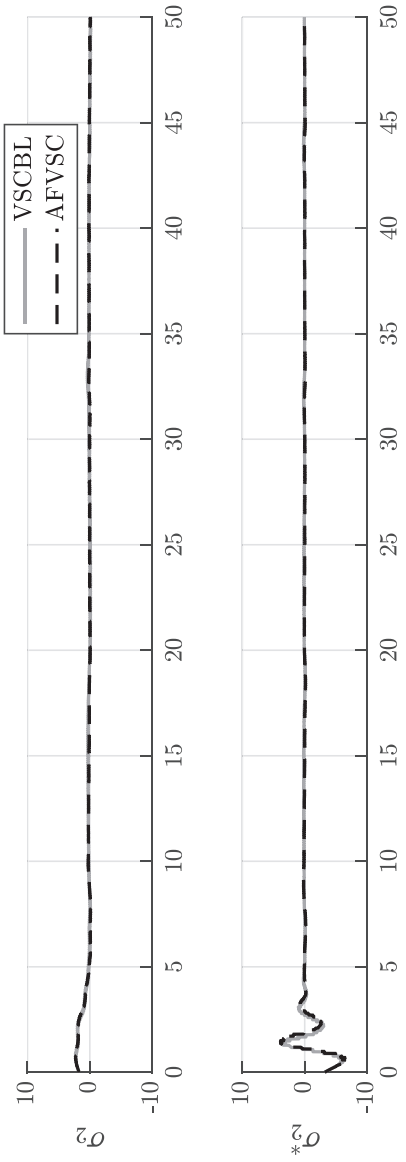

Figure 10. Sliding surface σ_2 and new sliding surface σ_2^* in the realistic scenario

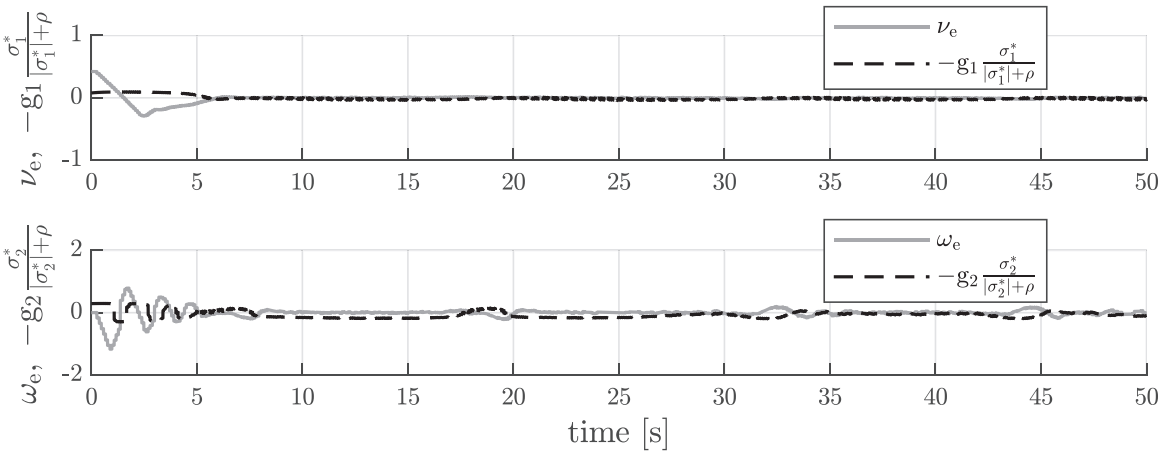

Figure 11. Auxiliary velocity tracking errors and compensations using VSCBL in the realistic scenario

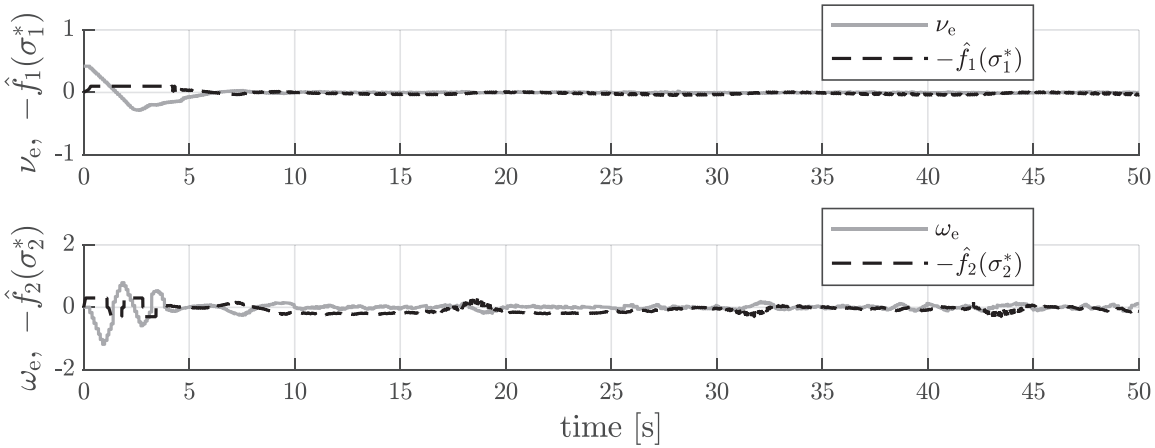

Figure 12. Auxiliary velocity tracking errors and compensations using AFVSC in the realistic scenario

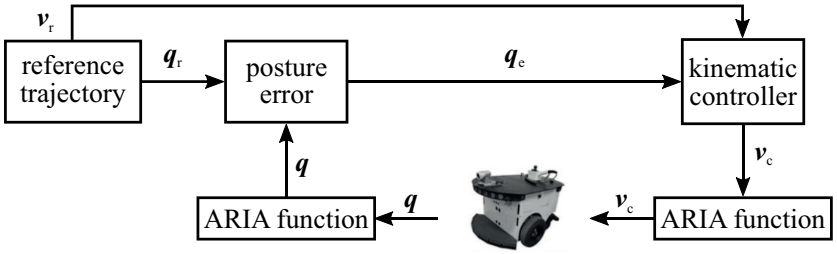

Figure 13. Block diagram of implementation in real time of experimental scenario

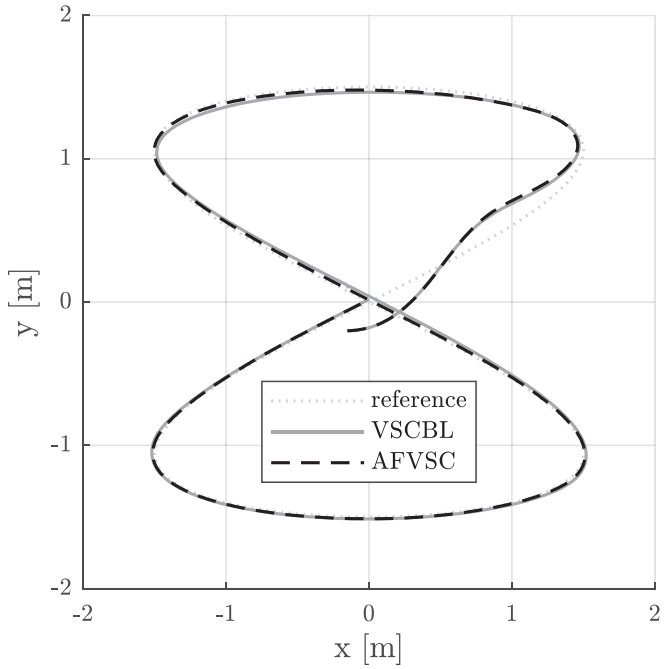

Figure 14. Trajectory tracking in the experimental scenario

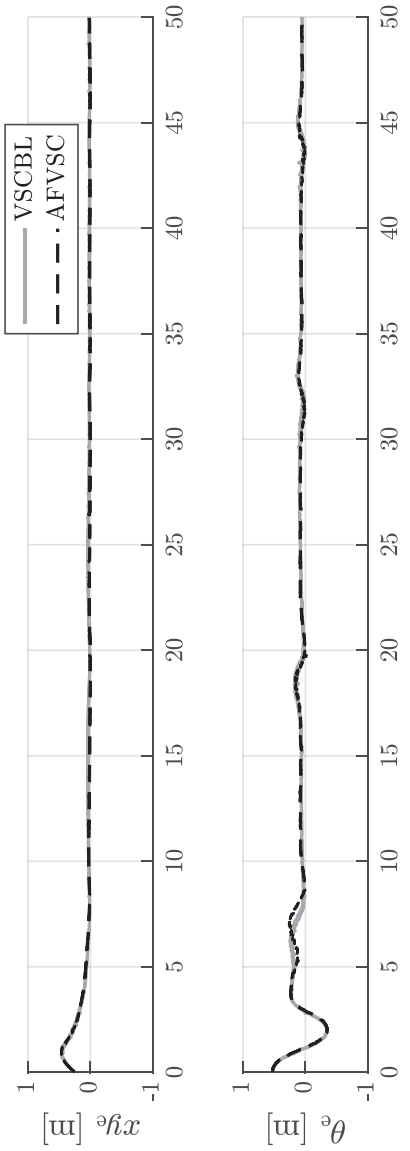

Figure 15. Posture tracking and orientation errors in the experimental scenario

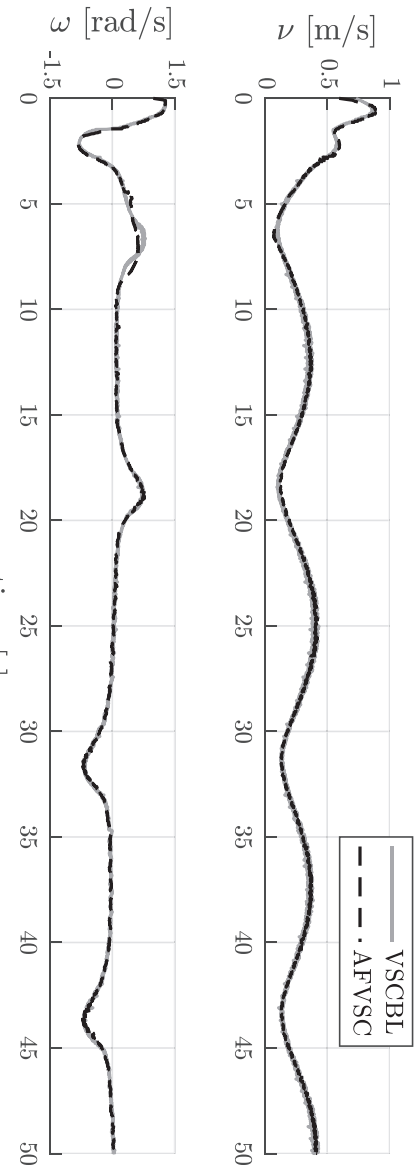

Figure 16. Control velocities in the experimental scenario

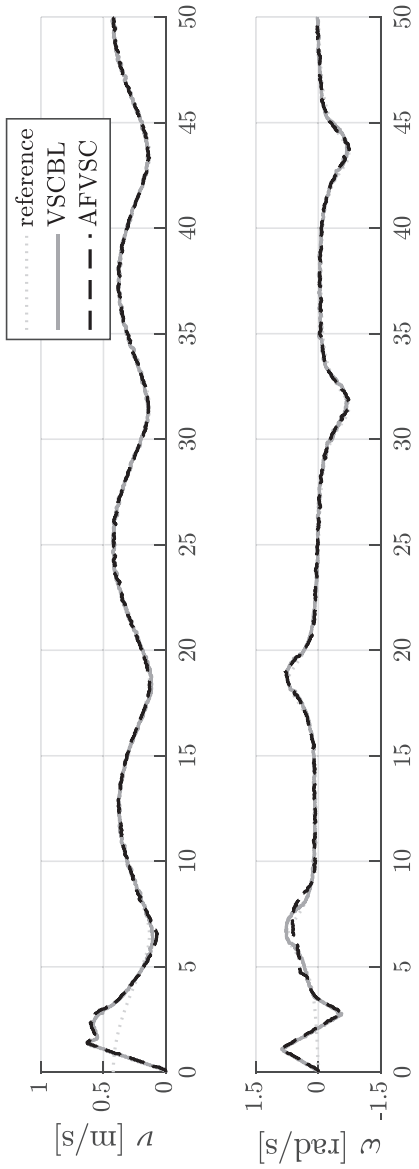

Figure 17. Velocities of the DWMR and reference velocities in the experimental scenario

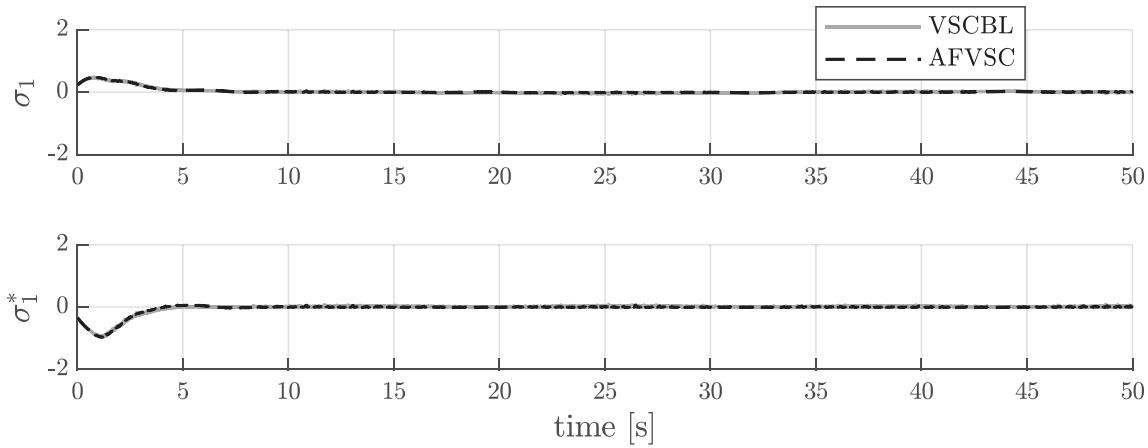

Figure 18. Sliding surface σ_1 and new sliding surface σ_1^* in the experimental scenario

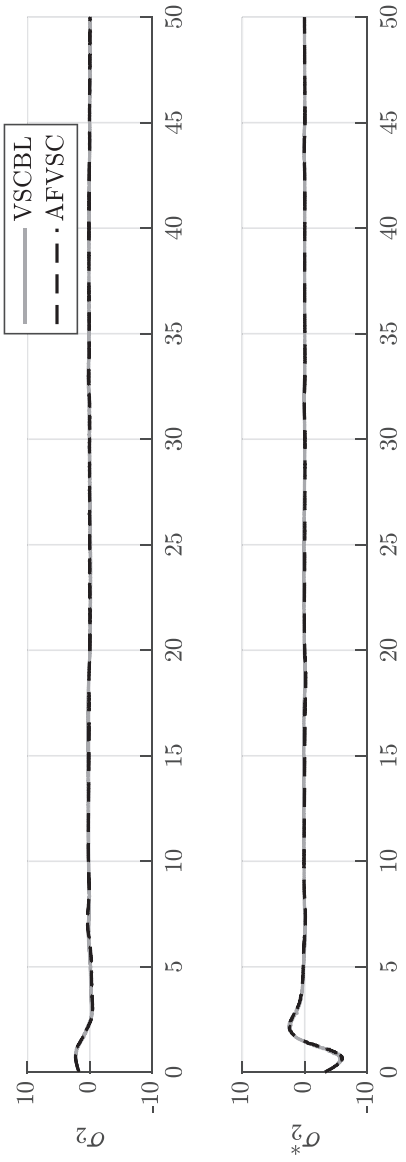

Figure 19. Sliding surface σ_2 and new sliding surface σ_2^* in the experimental scenario

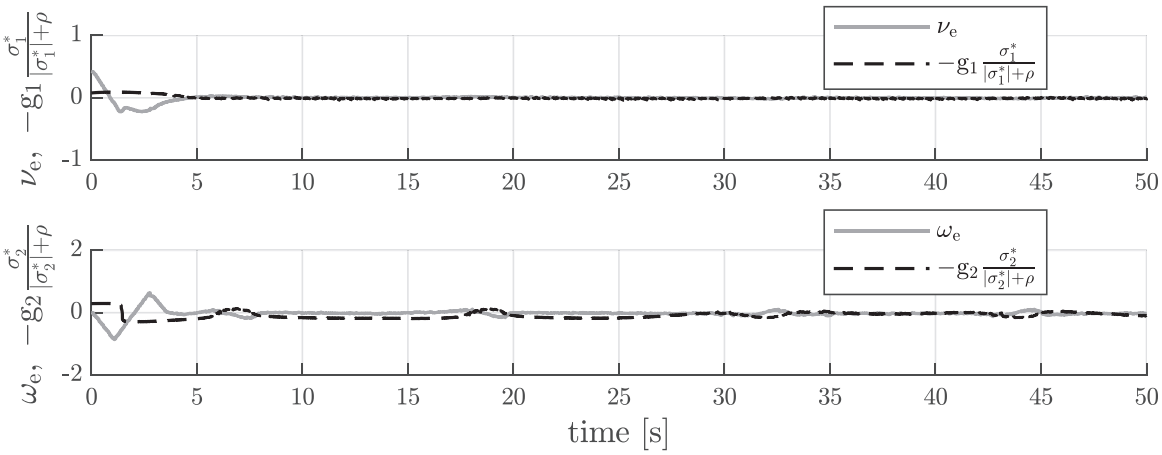

Figure 20. Auxiliary velocity tracking errors and compensations using VSCBL in the experimental scenario

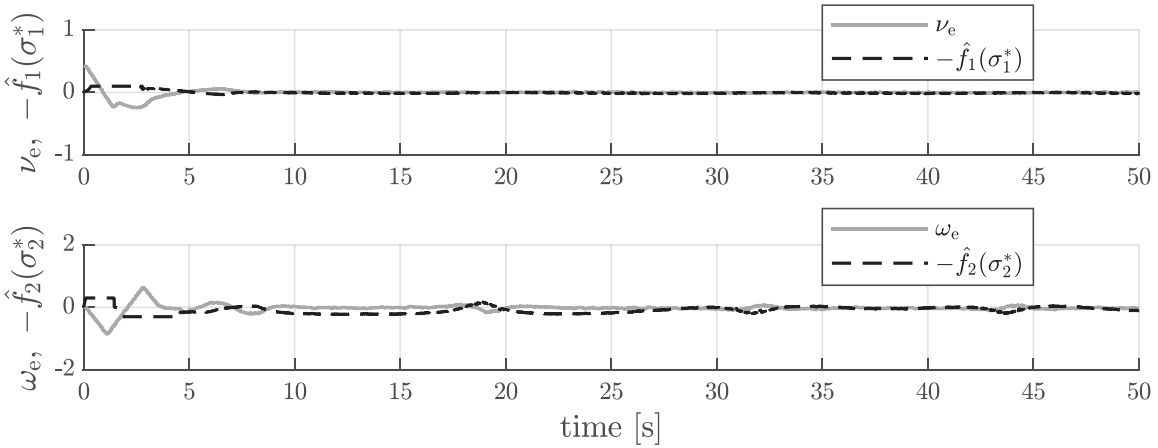

Figure 21. Auxiliary velocity tracking errors and compensations using AFVSC in the experimental scenario